

Enhanced Refocusing of Fat Signals Using Optimized Multipulse Echo Sequences

Ashley M. Stokes, Yesu Feng, Tanya Mitropoulos, and Warren S. Warren*

Endogenous magnetic resonance contrast based on the localized composition of fat in vivo can provide functional information. We found that the unequal pulse timings of the Uhrig's dynamical decoupling multipulse echo sequences significantly alter the signal intensity compared to conventional, equal-spaced Carr–Purcell–Meiboom–Gill sequences. The signal increases and decreases depending on the tissue and sequence parameters, as well as on the interpulse spacings; particularly strong differences were observed in fatty tissues, which have a highly structured morphology and a wide range of chemical shifts and J-couplings. We found that the predominant mechanism for fat refocusing under multipulse echo sequences is the chemical structure, with stimulated echoes playing a pivotal role. As a result, specialized pulse sequences can be designed to optimize refocusing of the fat chemical shifts and J-couplings, where the degree of refocusing can be tailored to specific types of fats. To determine the optimal time delays, we simulated various Uhrig dynamical decoupling and Carr–Purcell–Meiboom–Gill pulse sequence timings, and these results are compared to experimental results obtained on excised and in vivo fatty tissue. Applications to intermolecular multiple quantum coherence imaging, where the improved echo refocusing translates directly into signal enhancements, are presented as well. **Magn Reson Med** 69:1044–1055, 2013. © 2012 Wiley Periodicals, Inc.

Key words: multipulse echo sequences; strong coupling Hamiltonian; lipids

Endogenous magnetic resonance contrast based on the localized composition of fat in vivo can provide functional information. For example, by isolating the polyunsaturated lipid signal with a selective conventional multiple quantum coherence transfer technique, an absence of polyunsaturated fats was observed to correlate with invasive ductal carcinoma in the breast, whereas healthy breast tissue showed a continuous distribution of fats (1). Using intermolecular multiple quantum coherences (iMQCs), fat can be used to image absolute temperature in vivo (2,3) and detect brown adipose tissue (an important goal for obesity research) (4,5). However, the spectrum of fat has at least 10 distinct resonances and many J-couplings (6–9), in many cases between spins with

very similar resonance frequencies. Even at high fields, the dynamics in a spin echo (SE) sequence can be complex, as these frequencies can constructively and destructively interfere for different evolution times. As a result, some sequence delays are inherently better than others. Here, we show that specialized multipulse echo sequences can be designed to optimize refocusing of the chemical shifts and J-couplings in fat, where the degree of refocusing can be tailored for specific delays and echo times (TEs).

Carr–Purcell–Meiboom–Gill (CPMG) (10,11) multipulse echo sequences are well known to provide improved refocusing in tissue compared to standard SE sequences (12). The CPMG sequence uses equal interpulse delays, and it is easy to show that for diffusion in a constant gradient, this configuration gives the best signal for a fixed overall sequence length. However, we recently showed that, surprisingly, the equal pulse spacing of the CPMG sequence is not generally optimum for refocusing frequency fluctuations such as those found in vivo (13). For example, Fig. 1 shows a nonintuitive unequal spacing called the Uhrig dynamic decoupling (UDD) sequence (14). This sequence was initially proposed to reduce decoherence in an application unrelated to magnetic resonance, but it was later shown to be more general (15–18). For the UDD sequence, the j th pulse in an n -pulse sequence is located at a time given by $\delta_j = TE \left\{ \sin^2 \left(\frac{\pi j}{(2n+2)} \right) \right\}$. This unique timing led to significant increases in signal in many types of tissue (13). However, these improvements depend on the tissue and sequence parameters, as well as on the interpulse spacings; particularly strong enhancements were observed in fatty tissues, which have a highly structured morphology and a wide range of chemical shifts and J-couplings.

Human adipose tissue is composed mostly of triglycerides (19–22). Three fatty acids (oleic, palmitic, and linoleic) account for 77–89% of the fatty acids in vivo (6–9,19–22). The chemical structure of a typical fat molecule is shown in Fig. 2a. The typical fat molecule has 10 resolvable proton resonances (6–9), shown in Fig. 2b. Table 1 uses the conventional labeling scheme from A to J in alphabetical order starting from upfield to downfield. While not generally resolvable in vivo, this molecule also has J-couplings between adjacent spins. From the COSY spectrum in Fig. 2c, there is J-coupling between resonances A and B; B and C; B and D; C and E; D and J; F and J; and G and H, which provides good agreement with the molecule shown in Fig. 2a. These J-couplings are shown in Table 1, where the values were estimated using the incremental method in ChemBioDraw Ultra Version 12.0 (Cambridge Soft Corporation, Cambridge, MA) and provide good agreement with high resolution

Department of Chemistry, Center for Molecular and Biomolecular Imaging, Duke University, Durham, North Carolina, USA.

Grant sponsor: NIH; Grant number: EB 02122.

*Correspondence to: Warren S. Warren, Ph.D., Department of Chemistry, Center for Molecular and Biomolecular Imaging, Duke University, FFSC Box 90346, 124 Science Drive, Durham, NC 27708-0346. E-mail: warren.warren@duke.edu

Received 9 February 2012; revised 9 April 2012; accepted 24 April 2012.

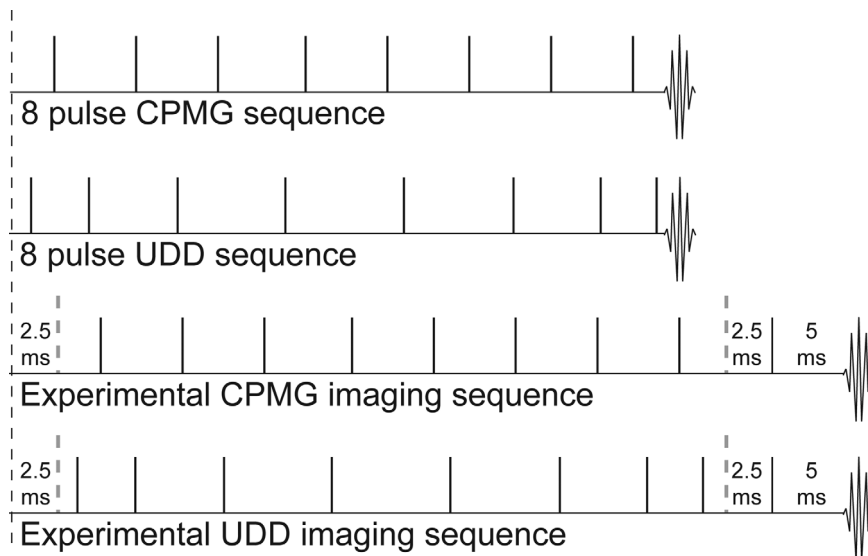
DOI 10.1002/mrm.24340

Published online 24 May 2012 in Wiley Online Library (wileyonlinelibrary.com).

© 2012 Wiley Periodicals, Inc.

1044

FIG. 1. Eight pulse CPMG (top) and UDD (upper middle) sequences. All pulses shown are π pulses, while the location of the $\pi/2$ excitation pulse in each sequence is indicated by the black dotted line. The CPMG sequence has equally spaced pulses, while the UDD sequence has shorter delays at the beginning and end and longer delays in the middle. The lower middle and bottom sequences show the timing for the experimental imaging sequences, where a SE sequence (TE = 10 ms) is added after the CPMG and UDD sequences to provide slice selection.



spectra of similar molecules (24,25). The three most common fatty acids can be differentiated by four resonances (B, D, F, and J) according to the number of saturated and unsaturated carbons. Fat and vegetable oil have nearly identical chemical structures and spectra (Fig. 2a); however, fat has a complex microstructure, which oil lacks. By considering both fat and oil, the effects of chemical structure and tissue structure can be separated, allowing us to determine the predominant mechanisms for refocusing.

In vivo applications typically involve many different components of varying spin complexity, from simple spin systems such as water to more complicated spin systems such as fat or metabolites. In the case of a single spin system (or a noncoupled multispin system), differences between multipulse echo sequences may be observed due to stimulated echoes and different spectral density profiles. More specifically, the CPMG sequence would have increased signal under stimulated echoes due to constructive interference patterns at the peak of the echo, while the UDD sequence provides improved refocusing compared to the CPMG sequence for low frequency fluctuations arising from diffusion or susceptibility (13). On the other hand, coupled multispin systems also exhibit echo modulations as a result of the J-couplings under multipulse echo sequences (26,27). In fast SE imaging, the fat voxels appear bright (27–32), known as the bright fat phenomenon, which was initially thought to be the result of increases in T_2 due to decreased J-coupling modulation of echo amplitudes. Other possible mechanisms for increased T_2 are diffusion and exchange effects, as well as stimulated echoes. These mechanisms have been investigated in detail by several groups (30,32–36), and stimulated echoes and chemical exchange were found to contribute negligibly (33). Henkelman et al. (30) found that diffusion may play a role in the bright fat signal, but the general consensus has been that the J-couplings play a significant role in refocusing.

The Hamiltonian for a coupled n -spin system in the rotating frame is given by

$$H = \sum_{i=1}^n \Omega_i I_{zi} + \sum_{i=1}^n \sum_{j<i}^n 2\pi J_{ij} I_i \cdot I_j$$

$$= \sum_i^n \Omega_i I_{zi} + \sum_{i=1}^n \sum_{j<i}^n 2\pi J_{ij} (I_{iz} I_{jz} + I_{ix} I_{jx} + I_{iy} I_{jy}),$$

where Ω_i is the chemical shift of spin i , and J_{ij} is the scalar coupling constant between spins i and j . The z component of the J-coupling term commutes with the chemical shift term; the x and y components of the J-coupling term, which permit mutual spin–spin flip-flops, do not commute with the difference between the chemical shifts of spins i and j . Thus, the x and y components are appropriately truncated (leaving only $2\pi J_{12} I_{1z} I_{2z}$ as the two-spin J-coupling term) for long time evolution in the weak coupling limit (i.e., when the chemical shift difference is much larger than the J-coupling constant). Because the phase evolution caused by the J-coupling is not reversed by π pulses, the signal is cosinusoidally modulated with zero values at TEs of $(2n + 1)/2J$, $n = 0, 1, 2, \dots$ (28). In the spectrum, the peaks will oscillate between antiphase for these TEs and in phase for TEs of $(2n + 1)/(J)$, $n = 0, 1, 2, \dots$. In principle, appropriate choice of the TE can accurately refocus the J-coupling and produce in-phase magnetization. Unfortunately, for more complex spectra, there is no single value for TE that can accurately refocus all J-couplings.

On the other hand, when the spin system does not satisfy the weak coupling limit, or when a series of RF pulses is applied rapidly (such that $|(\Omega_i - \Omega_j)\tau| \ll 1$, where τ is the interpulse interval), the full J-coupling term $2\pi J_{12} I_1 \cdot I_2$ must be considered (26,32,37). A fast series of π pulses yields the following average Hamiltonian:

$$H_{\text{strong}} = \sum_{i=1}^n \sum_{j<i}^n 2\pi J_{ij} I_i \cdot I_j$$

This strong coupling Hamiltonian is also called the isotropic mixing Hamiltonian and is responsible for the coherence transfer in total correlation spectroscopy (38) and in homonuclear Hartmann–Hahn spectroscopy (39).

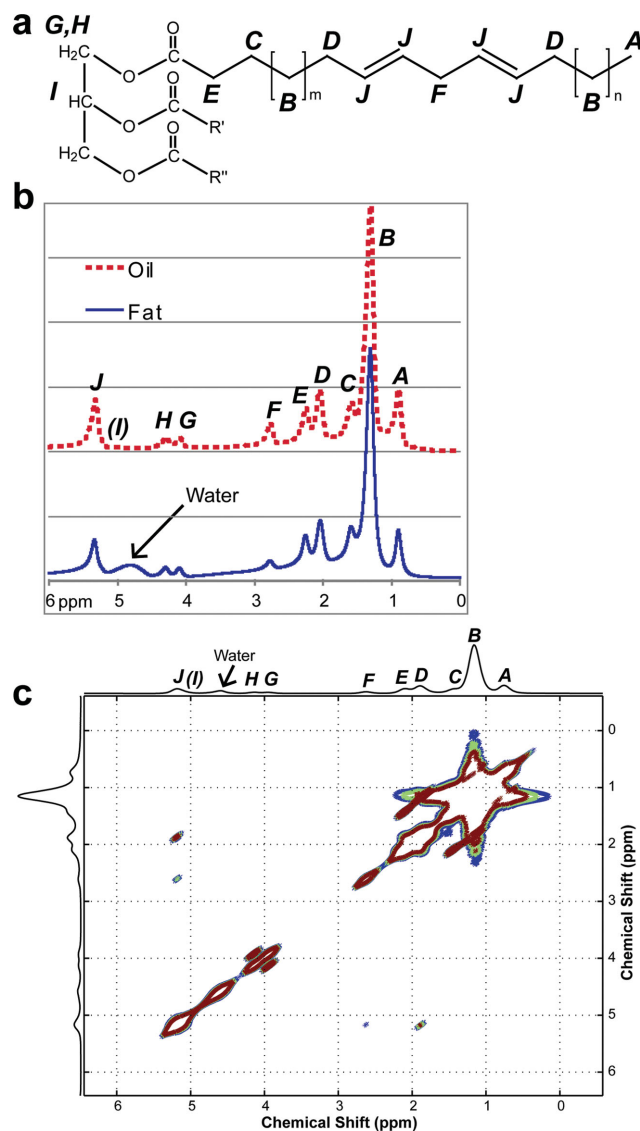


FIG. 2. **a**: The chemical structure of a typical fat molecule. **b**: ^1H NMR spectra of excised mouse fat (bottom trace) and vegetable oil (upper trace). Nine resonances can be resolved (A–J, excluding I, as labeled in **a**), and water signal is present in the mouse fat spectrum. **c**: COSY spectrum of excised mouse fat. J-couplings are present between spins A and B; B and C; B and D; C and E; D and J; F and J; G and H; G and I; and H and I. [Color figure can be viewed in the online issue, which is available at wileyonlinelibrary.com.]

Table 1
Chemical Shifts, Intensity Weighting Factors, and J-Coupling Values of Protons in Typical Fat Molecule (Shown in Fig. 2a)

Resonance	Functional group	Chemical shift (ppm) ^a	Weighting factor	J-coupling (Hz) ^a
A	CH ₃ methyl protons	0.90	9	AB = 8.0
B	CH ₂ methylene protons	1.29	60	BC = 7.1; BD = 7.1
C	CH ₂ methylene protons	1.64	6	CE = 7.1
D	CH ₂ allylic protons	2.18	12	DJ = 6.2
E	CH ₂ methylene protons	2.32	6	–
F	CH ₂ diallylic (bis-allylic) protons	2.63	6	FJ = ~1.0
G	CH ₂ glycerol backbone protons	4.20	2	GH = ~12.4; GI = 7.0
H	CH ₂ glycerol backbone protons	4.45	2	HI = 7.0
I	CH glycerol backbone protons	5.15	1	–
J	CH olefinic protons	5.45	12	–

^aFrom comparison of literature values (6,9,23), experimental 1D and 2D spectra, and ChemBioDraw spectral simulations.

Under this Hamiltonian, the individual spin operator I_{x1} can evolve to create the converse spin operator I_{x2} (and vice versa); however, these operators do not evolve independently (as is the case for weak coupling) but rather evolve as collective spin modes (32,38). In fact, because this Hamiltonian commutes with the total I_x or I_y , the total magnetization does not evolve under the strong coupling Hamiltonian, and the coupling between spins is *effectively* removed. Thus, for sufficiently short τ between π refocusing pulses, the J-coupling modulation that is characteristic of single-echo acquisitions will be suppressed. As a result, both fat and water are refocused for short TEs; experimentally, this causes the fat to appear bright in fast spin-echo images. However, for longer TEs, fat is poorly refocused.

Although stimulated echoes do not affect the T_2 contrast in fast spin-echo images, studies have found that the stimulated echoes do comprise a significant amount (up to 10%) of the overall signal (33,40). Whenever a series of π pulses ($n > 3$) is applied, stimulated echoes caused by pulse flip angle errors must be considered (33,41–43). Signal contributions from spurious pathways are highly probable in the CPMG and UDD sequences (which undoubtedly improves the CPMG signal for a single spin due to constructive interference patterns at the center of the echo). Although stimulated echoes can be used to increase the overall signal (44,45), refocusing away from the expected echo position inherently generates image distortion. Thus, many methods have been proposed to suppress stimulated echoes (41,42,46–48), and crusher gradients are the most effective of these methods. However, the situation becomes increasingly complicated for a J-coupled multispin system, and regimes may exist where the combined effects of stimulated echoes and J-coupling produce a null at the peak of the CPMG echo, while increasing the UDD signal.

In some cases, this enhanced fat signal is undesirable, and several methods have been proposed to obtain fast spin-echo image contrast that matches that of traditional SE methods (27,28,49–52). On the other hand, iMQC experiments such as temperature imaging (2,3) and brown fat detection (4,5) rely on the growth of signals with a fat component and are thus improved by better refocusing. In general, multipulse echo sequences have the potential to significantly improve the signal in multiple quantum sequences. More specifically, the pulse spacings can be modified to optimize refocusing of the

chemical shifts and J-couplings in fat, where the degree of refocusing can be tailored to specific types of fats. To determine the optimal time delays, computer simulations of a fat-like molecule will be used to explore the UDD and CPMG timings (by changing the TE or number of π pulses) for a 10-spin system, including effects of stimulated echoes due to imperfect π pulses. These results will be compared to localized spectroscopy and imaging of excised fatty tissue.

METHODS

Simulations

All simulation work was performed using Matlab software (Mathworks, Inc.). The density matrix evolution $\hat{\rho}(t)$ (37) in systems involving 10 spins was simulated under the effects of various sequences, including the conventional SE, double SE, CPMG and UDD with 4, 8, and 16 pulses. The input parameters for the simulation program were the number of spins (N), the proton chemical shifts and respective J-couplings, the sequence type and number of pulses, and the TE. The magnetic field strength was 7.05 T for all simulations unless otherwise noted. The chemical shifts and J-couplings were used to create the Hamiltonian operator, which is a $2^N \times 2^N$ matrix. All calculations were performed in the Hamiltonian eigenbasis, which was converted to the Zeeman basis to detect the final signal $\langle \hat{I}_x(t) - i\hat{I}_y(t) \rangle = \text{Tr}[\hat{\rho}(t)(\hat{I}_x - i\hat{I}_y)]$. Only the signal from the final echo was acquired for all simulations. For these simulations, T_2 relaxation was ignored. Moreover, all pulses were assumed to be instantaneous and produce exact 90° and 180° rotations. Simulations were also performed for the UDD and CPMG sequences with 170° and 175° pulses, which were averaged over a Gaussian resonance offset (FWHM = 1600 Hz), to determine the effects of stimulated echoes due to flip angle errors. In these simulations, 41 time points from immediately after the final 180° pulse to two times the final delay were acquired. The effects of crusher gradients were not considered in the simulations of stimulated echoes.

Simulations were performed on 1-pentene ($\text{CH}_3\text{CH}_2\text{-CH}_2\text{CH=CH}_2$) (10-spin system), which was chosen as a model for the lipid hydrocarbon chains, as previously shown by Stables et al. (27). The chemical shifts and J-couplings were estimated using the incremental method in ChemBioDraw Ultra Version 12.0 (Cambridge Soft Corporation, Cambridge, MA) and provided good agreement with previous results (27) and high resolution spectra of similar molecules (24,25). For these simulations, the absolute signal at the peak of the echo was determined for each sequence and TE, and the signal was normalized to the signal immediately after a 90° pulse.

For the simulations of a fat-like molecule, each resonance frequency (A through J) in the fat spectrum was used once for the chemical shifts inputs (for a total of 10 spins), while the J-couplings were estimated from comparisons of literature values (6,9,23,53), experimental 1D and 2D spectra, and spectral simulations using the incremental method in ChemBioDraw Ultra Version 12.0 (Cambridge Soft Corporation) (Table 1). The final signal

had significant splitting due to J-couplings, and line broadening was used to produce spectra that matched the experimental results. Finally, to obtain the correct intensities, each frequency was multiplied by the number of spins corresponding to that resonance in a typical fat molecule (see Table 1 for weighting factors).

Samples

All animal studies were performed in accordance with National Institutes of Health (NIH) Institutional Animal Care and Use Committee protocols as approved by Duke University. The obese mice were obtained from Jackson Laboratories (Bar Harbor, ME). Human breast tissue was obtained from anonymous healthy female patients undergoing breast reduction surgery. Institutional Review Board exemption was obtained for the use of human tissue.

Scan Parameters

Double SE, CPMG, and UDD sequences were used. For in vivo mouse imaging, the mouse was placed in a supine position, and axial slices through the abdomen or tumor were selected. For the human breast tissue, ~ 100 g of tissue was placed in a 50 mL centrifuge tube, which was used for the imaging. All MRI data were acquired on a Bruker 7.05 T (^1H : 300.5 MHz). Only the final echo was acquired for each pulse sequence, allowing fair comparisons between sequences of the same TE. Pulse positions for each sequence were calculated according to the aforementioned equations and are shown in Fig. 1. For the images, a 2-mm axial slice was selected with a $40 \text{ mm} \times 40 \text{ mm}$ FOV and 128×128 matrix size. Images were acquired with a TR of 1.5 s and 8 averages unless otherwise indicated. A 1 ms Hermite 90° pulse was used for excitation, and 1 ms hyperbolic secant (sech) 180° pulses were used for refocusing. Adiabatic pulses (such as sech) have significantly better RF homogeneity than conventional pulses but must be applied in identical pairs to compensate for the induced nonlinear phase of the transverse magnetization, where the phase reversal depends only on the formation of an echo and not on the individual delays (54–56). Slice selection was achieved with an extra 2 ms Hermite 180° pulse after the sequence (as discussed below). To reduce the effects of stimulated echoes, all 180° pulses were flanked by crusher gradients in different directions.

All images were processed using ImageJ (NIH, Bethesda, MD) and Matlab software (Mathworks, Inc.).

RESULTS

Simulation Results

Figure 3a shows the CPMG and UDD magnitude signals (relative to the free induction decay (FID) signal) for 1-pentene for a range of TEs. CPMG is shown in blue; and UDD is shown in red; simulations with 4, 8, and 16 pulses are shown on the left, middle, and right, respectively. The insets (below) show the typical experimental regime with TEs from 40 to 150 ms. As the number of pulses increases for each TE, the interpulse spacing decreases. While the differences between CPMG

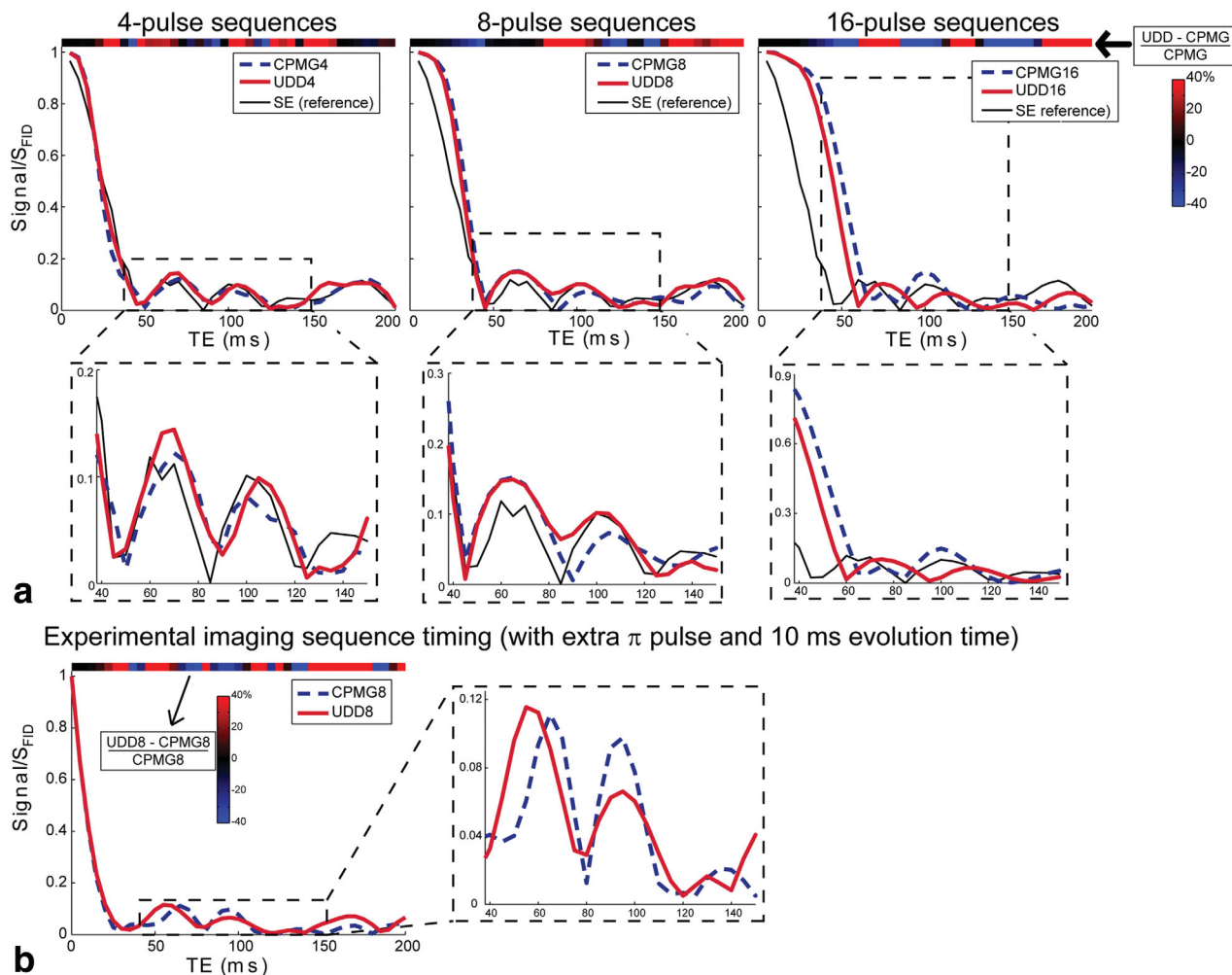


FIG. 3. **a**: Simulated echo signal for 1-pentene under SE and CPMG and UDD sequences with 4, 8, and 16 pulses, normalized to the FID signal. The inset regions (bottom) show the typical experimental TE regime, from 40 to 150 ms. J-couplings cause the signal to drop quickly (to $\sim 10\%$ after 45 ms), with subsequent signal oscillations. The color bar shown across the top of each graph shows the subtraction $(\text{UDD} - \text{CPMG})/\text{CPMG}$ and indicates the TEs where UDD is better and where CPMG is better. The optimal signal depends on the TE and number of pulses and is due to the complicated chemical structure of J-couplings. **b**: Simulated echo signal for 1-pentene under CPMG8 and UDD8 sequences using the timing of the experimental imaging sequence. The CPMG and UDD timings are calculated using the given TE (such that the echo spacing remains the same), but there is an extra π pulse after the final 180 to provide slice selection and an extra 10 ms of evolution time (2.5 ms before CPMG or UDD; 2.5 ms after CPMG or UDD; and 5 ms after the slice selective pulse). The inset region (right) shows the typical experimental TE regime, from 40 to 150 ms, and the color bar indicates $(\text{UDD} - \text{CPMG})/\text{CPMG}$. [Color figure can be viewed in the online issue, which is available at wileyonlinelibrary.com.]

and UDD seem small, the color bar at the top of each graph showing the subtraction $(\text{UDD} - \text{CPMG})/\text{CPMG}$ (%) shows significant differences between CPMG and UDD for the range of TEs. The optimal sequence timing (UDD or CPMG) depends strongly on the TE and reflects differences in the chemical shift and J-coupling refocusing.

Experimentally (where the minimum TE depends on pulse lengths, crusher gradients, and acquisition time), we have proposed a modification to the UDD and CPMG sequences that permits significantly shorter TEs: the placement of an extra echo pulse after the CPMG or UDD module to permit both slice selection and significantly shorter TEs (5 ms of evolution time was added before and after the pulse as well). Using this modified sequence, minimum TEs for the UDD sequence were 15

ms for 4 pulses, 35 ms for 8 pulses, and 145 ms for 16 pulses. Simulations of 1-pentene under this pulse sequence for UDD8 and CPMG8 (Fig. 3b) show that the signal drops off quickly, while the optimal sequence timing again depends strongly on the total TE (and thus interpulse spacing).

Even for a single spin, contributions from spurious pathways are highly probable in the CPMG and UDD sequences (which, without special care, manifest experimentally as banding artifacts in the UDD images). As a result of the unequal pulse spacings of the UDD sequence, its stimulated echoes refocus both before and after the primary echo. These extra echoes generally interfere with the primary echo in image space, producing bands of constructive and destructive interference in the resulting image. On the other hand, in the CPMG

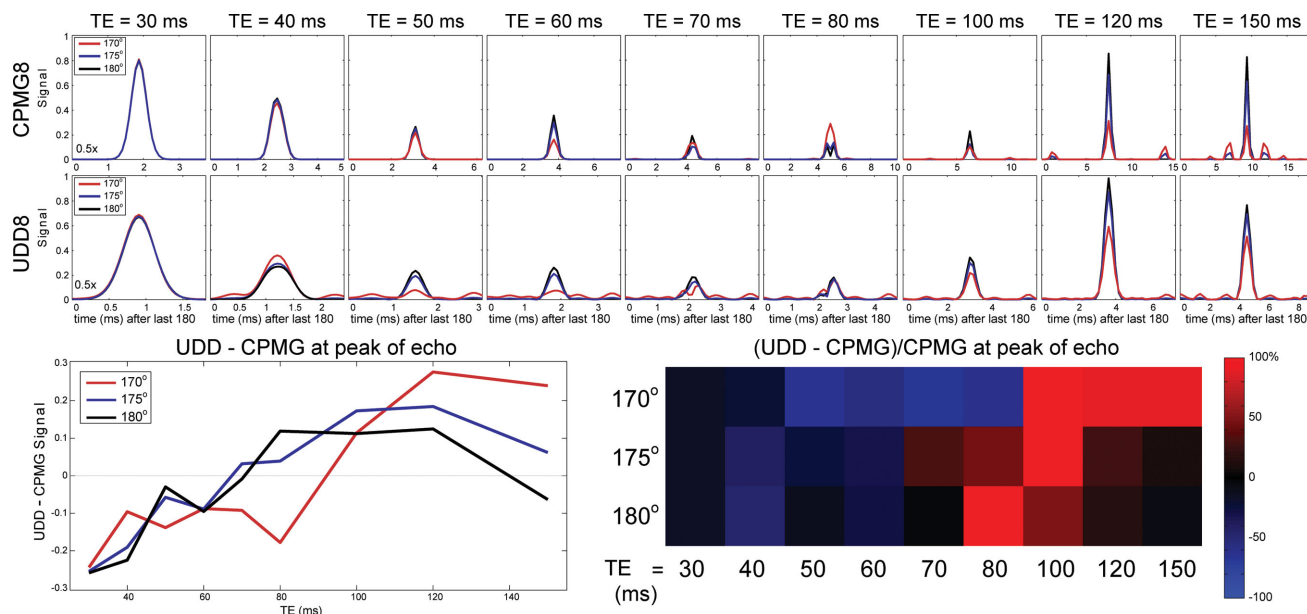


FIG. 4. Simulated echo signals for 1-pentene with 180° (perfect; black) pulses, 175° pulses (blue), and 170° pulses (red). RF inhomogeneity causes stimulated echoes, which alter the echo signal differently for CPMG and UDD. The different x-axis timescales for CPMG and UDD should be noted, which results from the shorter final UDD delay. The subtraction UDD – CPMG for the signal amplitude at the peak of the echo (bottom left) shows that the shorter TEs tend to favor the CPMG sequence, while the UDD sequence is favored at the longer TEs. This is also reflected in the image, normalized to the CPMG signal (bottom right). Even minor (<10%) RF inhomogeneity leads to significant changes in the optimal sequence for a given TE. [Color figure can be viewed in the online issue, which is available at wileyonlinelibrary.com.]

sequence, they are refocused concurrently with the primary echo and lead to images with enhanced intensity.

While the CPMG signal for a single-spin system will be increased due to stimulated echoes, the behavior is less certain when there are multiple spins and J-couplings. In these cases, stimulated echoes and J-coupling may combine to decrease the signal at the peak of the CPMG echo but to increase the UDD signal (although the opposite may also be true). The simulated signal for 1-pentene using CPMG8 and UDD8 sequences with pulse flip angles of 180° (perfect), 175°, and 170° for a range of TEs are shown in Fig. 4. The UDD echo appears earlier after the final pulse as a result of the shorter last delay compared to the CPMG sequence, and the different CPMG and UDD timescales should be noted (in other words, both the CPMG and UDD echoes are equally sharp). For perfect 180° pulses, the UDD8 signal is only higher than the CPMG8 signal for TEs between 80 and 120. However, for imperfect pulse flip angles (175° and 170°), the optimal sequence TEs shift, and the signal vs. time behavior for CPMG8 and UDD8 are complicated by both the stimulated echo and J-coupling modulation effects.

Simulations of a typical fat molecule were also performed by simplifying the fat molecule (shown in Fig. 2a) to a single proton for each individual chemical shift (for 10 simulated spins) and then postmultiplying the final signal by the number of protons (~130 actual spins) corresponding to each chemical shift. The simulated spectra of a fat molecule under the CPMG8 (in blue) and UDD8 (in red) sequences for a range of TEs are shown in Fig. 5. These spectra show that the shortest TEs do not

always have the highest signal intensity (T_2 relaxation has been ignored), and that the signal intensities oscillate with TE. Moreover, the optimal signal for each resonance depends on the pulse sequence and total TE, both of which relate to the interpulse spacings. Additionally, no single sequence type or TE provides the optimal signal for all resonances.

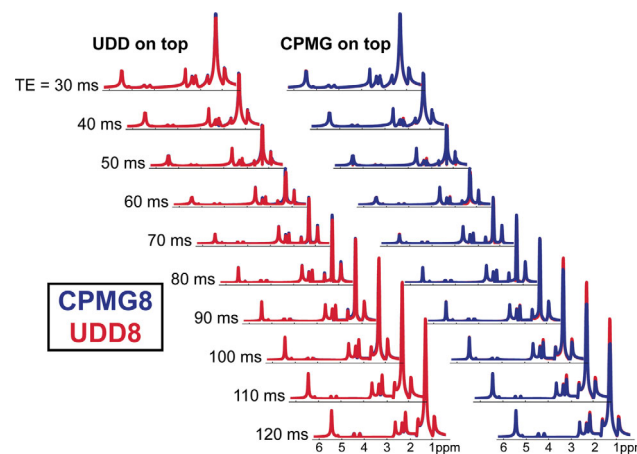


FIG. 5. Simulated CPMG8 and UDD8 spectra of a fat-like molecule for a range of TEs. On both the right and left, UDD8 is shown in red and CPMG8 is shown in blue. The left waterfall shows UDD plotted on top of CPMG and shows TEs and resonances where CPMG is better; the right waterfall shows CPMG plotted on top of UDD and shows TEs and resonances where UDD is better. [Color figure can be viewed in the online issue, which is available at wileyonlinelibrary.com.]

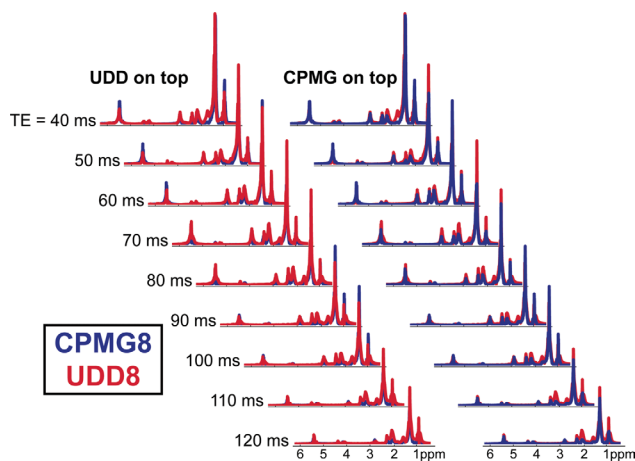


FIG. 6. CPMG8 and UDD8 localized spectroscopy of a tube of vegetable oil for a range of TEs. UDD8 is shown in red and CPMG8 is shown in blue. The left waterfall shows UDD plotted on top of CPMG8 and shows TEs and resonances where CPMG8 is better; the right waterfall shows CPMG8 plotted on top of UDD and shows TEs and resonances where UDD is better. [Color figure can be viewed in the online issue, which is available at wileyonlinelibrary.com.]

Experimental Results

The simulations show that the refocusing of fat depends strongly on the sequence type and total TE (and thus on the interpulse delays). Spectroscopy can be used to determine which resonances are optimally refocused for a given sequence and TE. Using a tube of vegetable oil as a simplified fat system, Fig. 6 shows the spectroscopy results from a voxel-selective modified PRESS sequence (eight selective pulses—three on the read direction, three on the phase direction, and two on the slice direction) with the CPMG (blue) and UDD (red) timings. The left side of the figure shows the resonances that the CPMG sequence refocuses better than the UDD sequence, while the right side shows resonances that the UDD sequence refocuses better than the CPMG sequence for a range of

TEs from 40 to 120 ms. For the A methyl peak, the CPMG and UDD sequences provide approximately equal refocusing for TEs 60 and 80 ms; CPMG is better than UDD for TEs 40, 90, and 100 ms; and UDD is better than CPMG for TEs 50, 70, 110, and 120 ms. For the B methylene peak, the CPMG and UDD sequences provide approximately equal refocusing for TEs 40 and 60 ms; CPMG is better than UDD for TEs 60, 90, and 100 ms; and UDD is better than CPMG for TEs 50, 70, 80, 110, and 120 ms. For the C methylene, D allylic, and E methylene peaks, the UDD sequence provides more refocusing than the CPMG sequence for all TEs shown. For the F diallylic peaks, the UDD sequence provides more refocusing than the CPMG sequence for the TEs less than 90 ms, while CPMG provides more signal for the longer TEs. The G and H peaks correspond to the glycerol backbone protons (along with the I proton, which was not observed here) and had too little signal intensity to easily discern the optimal sequence. The J olefinic peaks had approximately equal refocusing for the CPMG and UDD sequences for TEs 90, 100, 110, and 120 ms; CPMG provides better refocusing than UDD for TEs 40, 50, and 60 ms; and UDD is better than CPMG for TEs 70 and 80 ms. Improved refocusing of the individual resonances will be advantageous for iMQC imaging applications.

The strong signal dependence on the sequence type and total TE, both in the simulations and spectroscopy, illustrates the importance of the wide range of chemical shifts and J-couplings (6) (Fig. 2b); however, one can consider other mechanisms that could affect the signal refocusing, such as highly structured tissue morphology of fat leading to diffusion and exchange effects. To separate the chemical and tissue structure effects, we compared the CPMG and UDD images for oil and fat to elucidate the predominant mechanism for refocusing. Fat and oil have similar spectral characteristics, but oil lacks fat tissue microstructure. More specifically, similar signal characteristics for oil and fat would indicate that the chemical shifts and J-couplings are the predominant mechanism for signal refocusing, while different signal

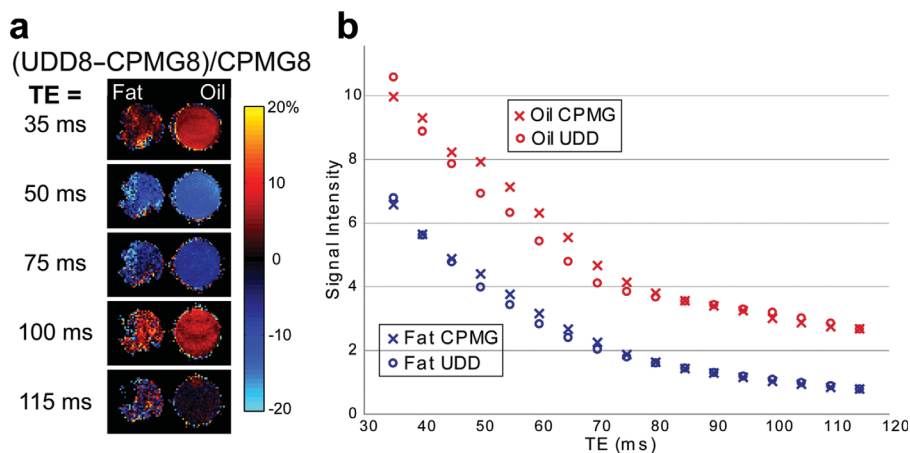


FIG. 7. **a**: Normalized subtraction images [(UDD8 – CPMG8)/CPMG8] for excised mouse fat and vegetable oil for several TEs. The oil and fat images have similar signal characteristics, which are due to chemical structure effects (as opposed to microstructure). **b**: Comparison of CPMG8 and UDD8 signal intensities for excised mouse fat and vegetable oil for a range of TEs (35–115 ms). [Color figure can be viewed in the online issue, which is available at wileyonlinelibrary.com.]

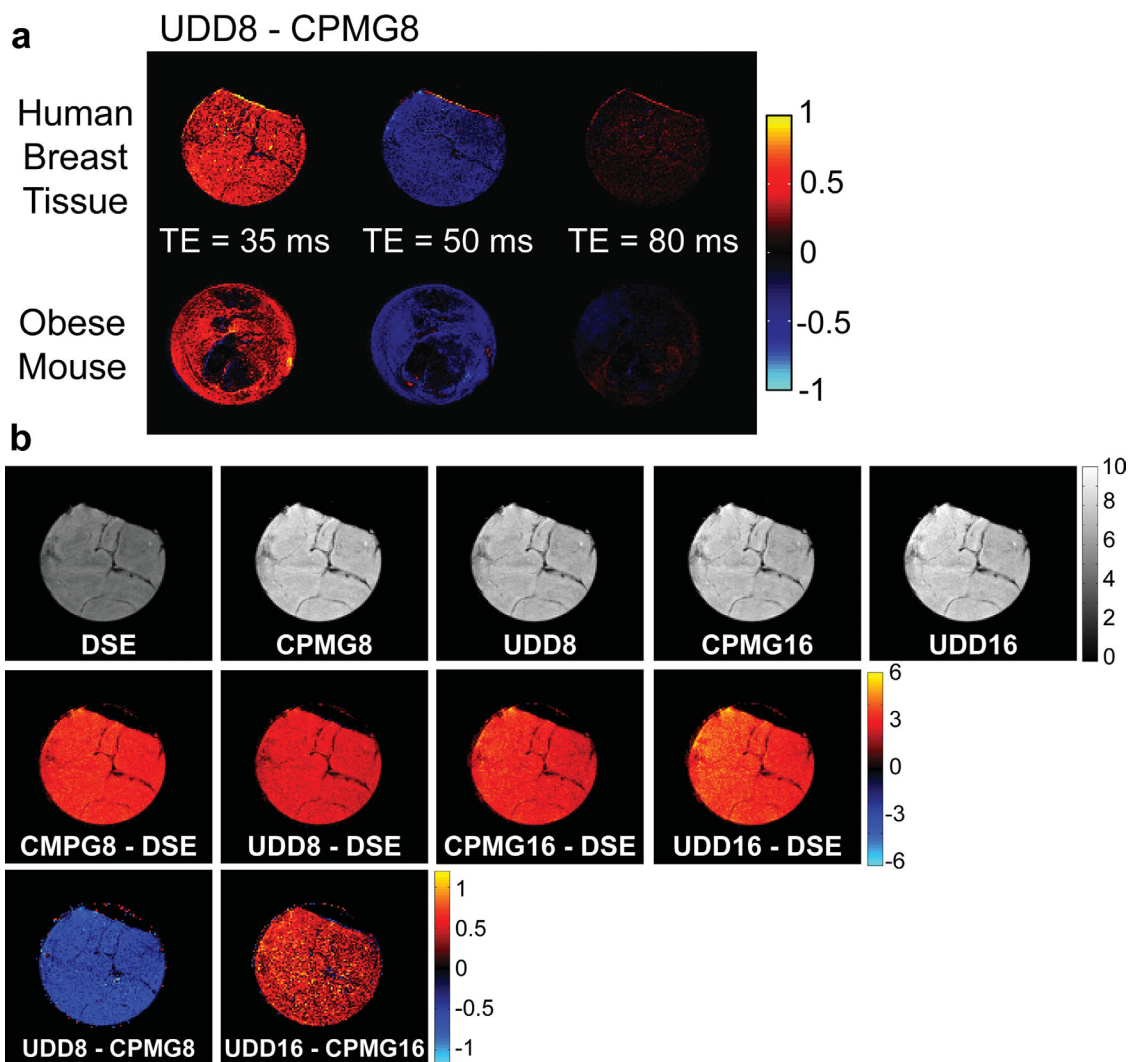


FIG. 8. **a**: Subtractions images for UDD8 – CPMG8 of excised human breast tissue (top) and obese mouse fat (bottom) for three TEs. **b**: Double SE, CPMG8, UDD8, CPMG16, and UDD16 images of excised human breast fat at TE = 120 ms. All CPMG and UDD sequences are better than the double SE sequence at this TE. However, CPMG8 is better than UDD8, while UDD16 is better than CPMG16 for refocusing the fat signal.

characteristics would indicate that the microstructure is the predominant mechanism. Moreover, this would allow us to determine whether vegetable oil is a fair test system for fat. Figure 7a compares the UDD and CPMG images for oil and fat and shows that the optimal sequence depends little on the microstructure, whereas the chemical shifts and J-couplings likely play a large role. This can also be seen in Fig. 7b for a wider range of TEs. The refocusing of fat depends strongly on the TE and thus on the interpulse delays, which results predominantly from chemical structure effects (with some contribution from tissue microstructure). Additionally, the similar characteristics show that vegetable oil can be used as a test system for fat. Careful timing of the interpulse delays should provide a mechanism to refocus more of these chemical shifts and J-couplings and thereby increase the signal.

Figure 8 shows the imaging results for CPMG8 and UDD8 in excised human breast tissue (top) and a post-

mortem obese mouse (bottom) for several TEs. These images show that the optimal TE for fat is different for CPMG8 and UDD8, where UDD8 outperforms CPMG8 at the shorter TE (35 ms) and CPMG8 outperforms UDD8 at the intermediate TE (50 ms), with about equal signals for UDD8 and CPMG8 at the longer TE (80 ms). Moreover, the optimal signal depends on the pulse sequence and total TE, indicating the importance of the interpulse spacings on the refocusing of the chemical shifts and J-couplings.

One goal in optimizing the pulse sequence and TE for fat refocusing is to apply these results to iMQC imaging of fat. Using the UDD8 and CPMG8 sequences following the iDQC-CRAZED (57–61) sequence on a tube of oil (which can be used as a simple model for fat chemical structure refocusing), we can determine the optimal sequence and TE. More specifically, Fig. 9 shows the oil tube subtraction images for (iDQC_UDD8 – iDQC_CPMG8)/iDQC_CPMG8 for a range of TEs from 40 to 120

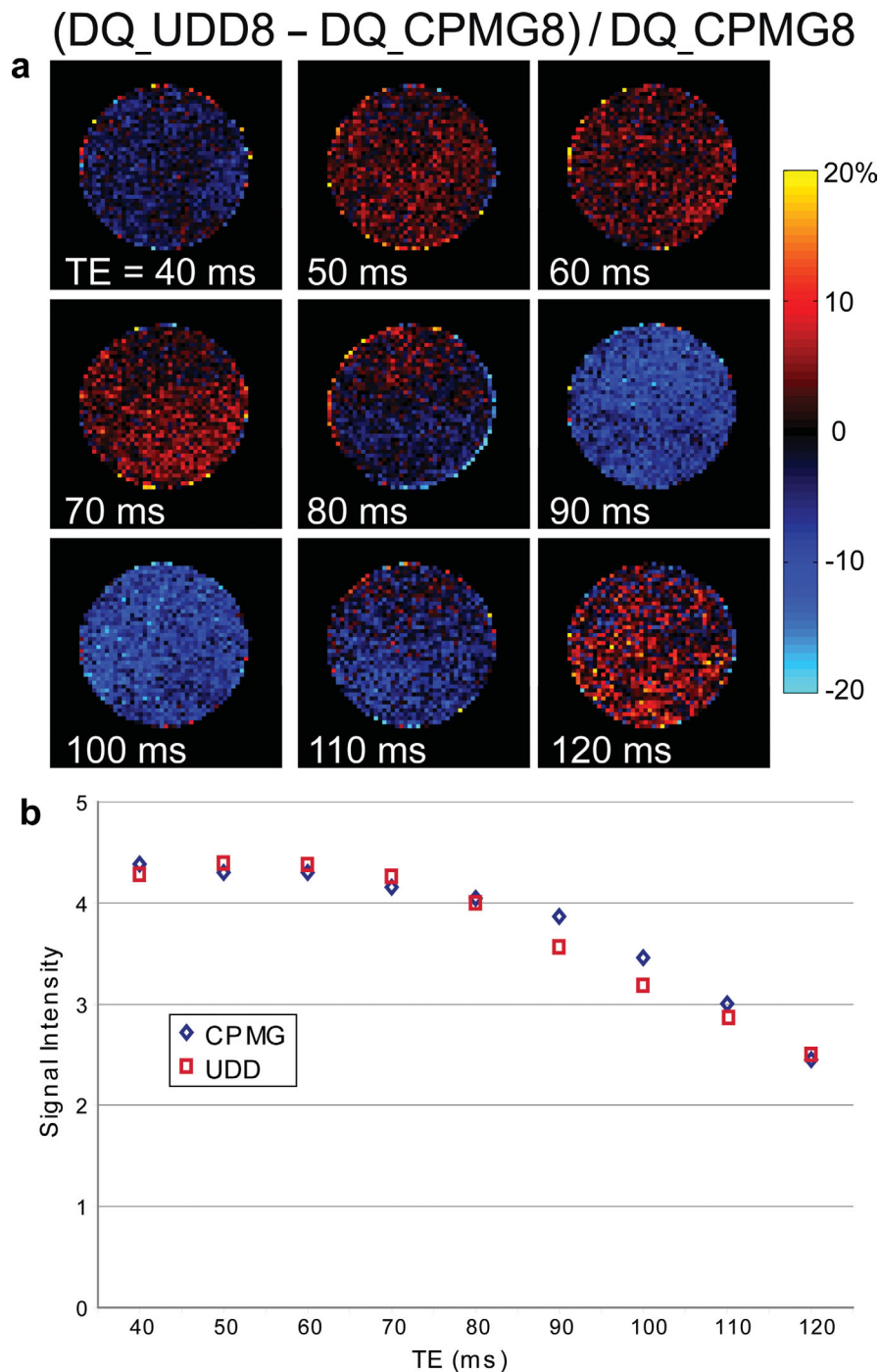


FIG. 9. **a**: Normalized subtraction images $[(\text{DQ_UDD8} - \text{DQ_CPMG8}) / \text{DQ_CPMG8}]$ for a tube of vegetable oil for a range of TEs. Similar to the conventional images, the optimal signal for iDQC followed by UDD8 or CPMG8 shows a strong dependence on the TE. **b**: Comparison of DQ_CPMG8 and DQ_UDD8 signal intensities for a tube of vegetable oil for a range of TEs (40–150 ms). [Color figure can be viewed in the online issue, which is available at wileyonlinelibrary.com.]

ms. Similar to the simulations and conventional imaging results, the optimal signal refocusing depends on the TE and sequence. Here, the CPMG and UDD sequences provide approximately equal refocusing for TE = 80 ms; CPMG is better than UDD at TEs 40, 90, 100, and 110 ms, and UDD is better than CPMG at TEs 50, 60, 70, and 120 ms. The combination of simulations, spectroscopy and imaging permits the optimization of refocusing for

fat under various pulse sequences and TEs; moreover, the optimal refocusing of fat will aid in iMQC imaging applications.

DISCUSSION

The simulation results show that the signal intensity resulting from the CPMG and UDD sequences depends

strongly on the TE and thus interpulse delays, which reflects differences in the refocusing of J-couplings. Using simulations of 1-pentene, the important parameters for refocusing are the chemical shift difference and J-coupling constant, as well as the sequence and total TE (both of which determine the interpulse spacings). With the strong J-coupling of 1-pentene (and thus fat), the initial signal intensity decreases quickly, with oscillations and periodic signal recurrences. As shown previously (26,27), as the chemical shift difference decreases, the J-coupling becomes less effective at dephasing the lipid signal. Thus, at lower magnetic fields (corresponding to smaller chemical shift difference frequencies), the dephasing ability of the J-coupling is significantly reduced (although the J-coupling constants result from the molecular magnetic properties and thus do not depend on the external magnetic field). Simulations of the pulse sequence used for the UDD8 and CPMG8 imaging experiments show that the signal drops off quickly, while the optimal TE depends strongly on the total TE (and thus interpulse spacing). Moreover, stimulated echoes resulting from imperfect refocusing pulses complicate the signal behavior for the different sequences. Even for relatively small pulse flip angle errors, the signal changes dramatically (most notably for CPMG8 at TE = 150 ms and UDD8 at TE = 60 ms). The optimal sequence timing (UDD or CPMG) depends strongly on the chemical shift differences, TEs, and J-couplings, indicating the lack of a global optimum for refocusing.

Using a tube of vegetable oil as a model system for fat, spectroscopy was used to determine which resonances are optimally refocused for a given sequence and TE. The refocusing of each peak was found to depend strongly on the TE and sequence; in other words, neither sequence can optimally refocus all resonances at all TEs. While the simulations show the importance of the wide range of chemical shifts and J-couplings, other mechanisms should also be considered, including the highly structured tissue morphology of fat leading to diffusion and exchange effects. Comparisons of CPMG and UDD images for oil and fat revealed that the refocusing of both samples predominantly results from chemical structure effects (with some contribution from tissue microstructure). Images were acquired using the CPMG8 and UDD8 sequences for a range of TEs in a postmortem obese mouse and excised human breast tissue. In both fat samples, the optimal signal depended on the pulse sequence and total TE, indicating the importance of the interpulse spacings on the refocusing of the chemical shifts and J-couplings. Similarly, iMQC images of vegetable oil were acquired and show significant differences in refocusing between the CPMG and UDD sequences (applied after the iDQC sequence) for different TEs. The addition of these multipulse echo sequences after the iDQC sequence provides time for the signals to grow in. The combination of simulations, spectroscopy and imaging permits the optimization of refocusing for fat under various pulse sequences and TEs; moreover, the optimal refocusing of fat will aid in iMQC imaging applications.

There are some limitations of this study. Although the simulated and experimental results are qualitatively similar, they are quantitatively different and can only show

which mechanisms and parameters will affect the signal. Most of the simulations (with the exception of Fig. 3b) lacked an extra π pulse and 10 ms delay present in the imaging sequences, and this could be a major source of discordance between the simulated and experimental results. While 1-pentene can provide some insight into the behavior of fat spins under multipulse echo sequences, it can only model the spin topology for the last few protons in the lipid chain and cannot yield any information for the other spins. The 10-spin simulation of the fat-like molecule makes several assumptions and simplifications, and we lack precise knowledge of the coupling constants, which were estimated from known hydrocarbon chains and using incremental method software. Moreover, the effects of J-coupling may be altered to various degrees by stimulated echoes, which we account for in the simulations, or by diffusion, chemical exchange effects, or coherence transfer crossrelaxation phenomena, which are not accounted for in the simulations (27,31). In addition, the simulations ignore all relaxation effects, including the known differential relaxation rates between protons in the hydrocarbon chain. Experimentally, vegetable oil is not a perfect model for fat. Over 90% of human fat is composed of seven fatty acids (which have different carbon chain lengths and numbers of double bonds); the predominant fatty acids are oleic (45–50%), palmitic (19–24%), and linoleic (13–15%), with the remaining myristic, palmitoleic, stearic, and linolenic fatty acids accounting for another 13–18% (6). While vegetable oil can also contain these fatty acids, the composition of oil is different. Strictly speaking, the pulse repetition rate may not fall in the strong coupling (fast pulse) limit, especially for the longer TEs. However, an intermediate regime may exist between the strong and weakly coupled limits (27), and in fact, the UDD sequence results may be more difficult to interpret because of the changing interpulse delays (which are shorter at the beginning and end and longer in the middle of the sequence, as opposed to CPMG that has equidistant spacing between pulses). Finally, the effect of the strong coupling Hamiltonian depends on the offsets and chemical shifts (32,62), further complicating the comparisons between the simulation and experimental results.

CONCLUSION

We have demonstrated through density matrix simulations and experiments using an oil phantom and fatty tissue samples that J-couplings play a significant role in refocusing fat under multipulse echo sequences. Moreover, comparisons of oil and fat images reveal that microstructure, which includes the effects of diffusion and exchange, likely plays a negligible role in the refocusing, while the chemical structure and J-couplings are the predominant mechanism for refocusing. Density matrix simulations can be used to optimize the signal refocusing for a particular TE or resonance. The experimental results on vegetable oil provided good agreement with the simulations of 1-pentene, where the signal intensity depends on the sequence and number of pulses, as well as total TE. These results show that the conventional equally spaced CPMG sequence is not the global

optimal timing, although the optimal timing to refocus J-couplings may not be the UDD sequence either. The simulation, spectroscopy, and imaging results will enable the tailoring of specialized pulse sequences with optimized interpulse delays aimed at improving the refocusing of the fat signal. This increased fat signal will ultimately prove useful for iMQC applications that rely on the growth of signals with a fat component.

ACKNOWLEDGMENTS

A.M.S. thanks Dr. R.T. Branca for helpful discussion. The authors acknowledge Dr. S. Hollenbeck for providing the excised tissue samples.

REFERENCES

- He QH, Shkarin P, Hooley RJ, Lannin DR, Weinreb JC, Bossuyt VJ. In vivo MR spectroscopic imaging of polyunsaturated fatty acids (PUFA) in healthy and cancerous breast tissues by selective multiple-quantum coherence transfer (Sel-MQC): a preliminary study. *Magn Reson Med* 2007;58:1079–1085.
- Galiana G, Branca RT, Jenista ER, Warren WS. Accurate temperature imaging based on intermolecular coherences in magnetic resonance. *Science* 2008;322:421–424.
- Jenista E, Galiana G, Branca RT, Yarmolenko PS, Stokes AM, Dewhirst MW, Warren WS. Application of mixed spin iMQCs for temperature and chemical-selective imaging. *J Magn Reson* 2010;204:208–218.
- Branca RT, Warren WS. In vivo brown adipose tissue detection and characterization using water-lipid intermolecular zero-quantum coherences. *Magn Reson Med* 2010;65:313–319.
- Branca RT, Warren WS. In vivo NMR detection of diet-induced changes in adipose tissue composition. *J Lipid Res* 2011;52:833–839.
- Ren JM, Dimitrov I, Sherry AD, Malloy CR. Composition of adipose tissue and marrow fat in humans by H-1 NMR at 7 Tesla. *J Lipid Res* 2008;49:2055–2062.
- Knothe G, Kenar JA. Determination of the fatty acid profile by H-1-NMR spectroscopy. *Eur J Lipid Sci Technol* 2004;106:88–96.
- Miyake Y, Yokomizo K, Matsuzaki N. Determination of unsaturated fatty acid composition by high-resolution nuclear magnetic resonance spectroscopy. *J Am Oil Chem Soc* 1998;75:1091–1094.
- Yeung DKW, Lam SL, Griffith JF, Chan ABW, Chen Z, Tsang PH, Leung PC. Analysis of bone marrow fatty acid composition using high-resolution proton NMR spectroscopy. *Chem Phys Lipids* 2008;151:103–109.
- Carr HY, Purcell EM. Effects of diffusion on free precession in nuclear magnetic resonance experiments. *Phys Rev* 1954;94:630–638.
- Meiboom S, Gill D. Modified spin-echo method for measuring nuclear relaxation times. *Rev Sci Instrum* 1958;29:688–691.
- Michaeli S, Grohn H, Grohn O, Sorce DJ, Kauppinen R, Springer CS, Ugurbil K, Garwood M. Exchange-influenced T-2p contrast in human brain images measured with adiabatic radio frequency pulses. *Magn Reson Med* 2005;53:823–829.
- Jenista ER, Stokes AM, Branca RT, Warren WS. Optimized, unequal pulse spacing in multiple echo sequences improves refocusing in magnetic resonance. *J Chem Phys* 2009;131:204510–204517.
- Uhrig GS. Keeping a quantum bit alive by optimized Pi-pulse sequences. *Phys Rev Lett* 2007;98:100504–100508.
- Biercuk MJ, Uys H, van Devender AP, Shiga N, Itano WM, Bollinger JJ. Optimized dynamical decoupling in a model quantum memory. *Nat Lett* 2009;458:996–1000.
- Cywinski L, Lutchny RM, Nave CP, Das Sarma S. How to enhance dephasing time in superconducting qubits. *Phys Rev B* 2008;77:174509–174520.
- Yang W, Liu RB. Universality of Uhrig dynamical decoupling for suppressing qubit pure dephasing and relaxation. *Phys Rev Lett* 2008;101:180403–180407.
- Lee B, Witzel WM, Das Sarma S. Universal pulse sequence to minimize spin dephasing in the central spin decoherence problem. *Phys Rev Lett* 2008;100:160505–160509.
- Kokatnur MG, Oalman MC, Johnson WD, Malcom GT, Strong JP. Fatty-acid composition of human adipose-tissue from 2 anatomical sites in a biracial community. *Am J Clin Nutr* 1979;32:2198–2205.
- Field CJ, Angel A, Clandinin MT. Relationship of diet to the fatty-acid composition of human adipose-tissue structural and stored lipids. *Am J Clin Nutr* 1985;42:1206–1220.
- Insull W, Bartsch GE. Fatty acid composition of human adipose tissue related to age sex and race. *Am J Clin Nutr* 1967;20:13–23.
- Malcom GT, Bhattacharyya AK, Velezduan M, Guzman MA, Oalman MC, Strong JP. Fatty-acid composition of adipose-tissue in humans—differences between subcutaneous sites. *Am J Clin Nutr* 1989;50:288–291.
- Oostendorp M, Engelke UFH, Willemsen MAA, Wevers RA. Diagnosing inborn errors of lipid metabolism with proton nuclear magnetic resonance spectroscopy. *Clin Chem* 2006;52:1395–1405.
- Pouchert CJ, Aldrich Chemical C, Behnke J. The Aldrich library of ¹³C and ¹H FT NMR spectra. Milwaukee, WI: Aldrich Chemical, Co.; 1993.
- Bothner-By AA, Naar-Colin C. The proton magnetic resonance spectra of olefins. I. Propene, butene-1 and hexene-1. *J Am Chem Soc* 1961;83:231–236.
- Allerhand A. Analysis of Carr-Purcell Spin-Echo NMR experiments on multiple-spin systems. I. Effect of homonuclear coupling. *J Chem Phys* 1966;44:1–9.
- Stables LA, Kennan RP, Anderson AW, Constable RT, Gore JC. Analysis of J coupling-induced fat suppression in DIET imaging. *J Magn Reson* 1999;136:143–151.
- Constable RT, Smith RC, Gore JC. Coupled-spin fast spin-echo MR-imaging. *JMRI-J Magn Reson Imag* 1993;3:547–552.
- Gambarota G, van der Graaf M, Klomp D, Mulkern RV, Heerschap A. Echo-time independent signal modulations using PRESS sequences: a new approach to spectral editing of strongly coupled AB spin systems. *J Magn Reson* 2005;177:299–306.
- Henkelman RM, Hardy PA, Bishop JE, Poon CS, Plewes DB. Why fat is bright in rare and fast spin-echo imaging. *JMRI-J Magn Reson Imag* 1992;2:533–540.
- Stables LA, Kennan RP, Anderson AW, Gore JC. Density matrix simulations of the effects of J coupling in spin echo and fast spin echo imaging. *J Magn Reson* 1999;140:305–314.
- Williamson DS, Mulkern RV, Jakab PD, Jolesz FA. Coherence transfer by isotropic mixing in Carr-Purcell-Meiboom-Gill imaging: implications for the bright fat phenomenon in fast spin-echo imaging. *Magn Reson Med* 1996;35:506–513.
- Constable RT, Anderson AW, Zhong J, Gore JC. Factors influencing contrast in fast spin-echo MR imaging. *Magn Reson Imag* 1992;10:497–511.
- Melki PS, Jolesz FA, Mulkern RV. Partial RF echo-planar imaging with the Faise method. II. Contrast equivalence with spin-echo sequences. *Magn Reson Med* 1992;26:342–354.
- Melki PS, Mulkern RV. Magnetization transfer effects in multislice rare sequences. *Magn Reson Med* 1992;24:189–195.
- Wright GA, Macovski A. Lipid Signal Enhancement in Spin-Echo Trains. In: Proceedings of the 11th Annual Meeting of ISMRM, Berlin, Germany, 1992. p. 437.
- Slichter CP. Principles of magnetic resonance. New York: Springer-Verlag; 1990.
- Braunschweiler L, Ernst RR. Coherence transfer by isotropic mixing—Application to proton correlation spectroscopy. *J Magn Reson* 1983;53:521–528.
- Davis DG, Bax A. Assignment of complex H-1-NMR spectra via two-dimensional homonuclear Hartmann-Hahn spectroscopy. *J Am Chem Soc* 1985;107:2820–2821.
- Hennig J, Nauwerth A, Friedburg H. Rare imaging—a fast imaging method for clinical MR. *Magn Reson Med* 1986;3:823–833.
- Zur Y, Stokar S. A phase-cycling technique for canceling spurious echoes in NMR imaging. *J Magn Reson* 1987;71:212–228.
- Zur Y, Zou X, Neuringer LJ. Multiecho, spin-echo sequence to eliminate unwanted echoes. *Magn Reson Med* 1991;19:464–469.
- Crawley AP, Henkelman RM. A stimulated echo artifact from slice interference in magnetic-resonance-imaging. *Med Phys* 1987;14:842–848.
- Melki PS, Mulkern RV, Panych LP, Jolesz FA. Comparing the Faise method with conventional dual-echo sequences. *JMRI-J Magn Reson Imag* 1991;1:319–326.
- Constable RT, Smith RC, Gore JC. Signal-to-noise and contrast in fast spin-echo (FSE) and inversion recovery FSE imaging. *J Comput Assist Tomogr* 1992;16:41–47.
- Crawley AP, Henkelman RM. Errors in T2 estimation using multislice multiple-echo imaging. *Magn Reson Med* 1987;4:34–47.

47. Majumdar S, Orphanoudakis SC, Gmitro A, Odonnell M, Gore JC. Errors in the measurements of T2 using multiple-echo MRI techniques .1. Effects of radiofrequency pulse imperfections. *Magn Reson Med* 1986;3:397–417.
48. Poon CS, Henkelman RM. Practical T2 quantitation for clinical-applications. *JMRI-J Magn Reson Imag* 1992;2:541–553.
49. Butts K, Pauly JM, Glover GH, Pelc NJ. Dual Echo “DIET” Fast Spin Echo Imaging. In: *Proceedings of the 3rd Annual Meeting of ISMRM, Nice, France, 1995*. p. 651.
50. Kanazawa H, Takai H, Machida Y, Hanawa M. Contrast naturalization of fast spin echo imaging: a fat reduction technique free from field inhomogeneity. In: *Proceedings of the 2nd Annual Meeting of ISMRM, San Francisco, CA, USA, 1994*. p. 474.
51. Kanazawa H, Miyazaki M, Takai H, Kassai Y, Hanawa M. A new fat-suppressed fast spin echo technique using DIET-PASTA. In: *Proceedings of the 4th Annual Meeting of ISMRM, New York, NY, USA, 1996*. p. 1547.
52. Block W, Pauly J, Kerr A, Nishimura D. Consistent fat suppression with compensated spectral-spatial pulses. *Magn Reson Med* 1997;38:198–206.
53. Strobel K, van den Hoff J, Pietzsch J. Localized proton magnetic resonance spectroscopy of lipids in adipose tissue at high spatial resolution in mice in vivo. *J Lipid Res* 2008;49:473–480.
54. Garwood M, DelaBarre L. The return of the frequency sweep: designing adiabatic pulses for contemporary NMR. *J Magn Reson* 2001;153:155–177.
55. Conolly S, Glover G, Nishimura D, Macovski A. A reduced power selective adiabatic spin-echo pulse sequence. *Magn Reson Med* 1991;18:28–38.
56. Hwang TL, Shaka AJ. Water suppression that works—excitation sculpting using arbitrary wave-forms and pulsed-field gradients. *J Magn Reson Ser A* 1995;112:275–279.
57. He QH, Richter W, Vathyam S, Warren WS. Intermolecular multiple-quantum coherences and cross correlations in solution nuclear-magnetic-resonance. *J Chem Phys* 1993;98:6779–6800.
58. Warren WS, Richter W, Andreotti AH, Farmer BT. Generation of impossible cross-peaks between bulk water and biomolecules in solution NMR. *Science* 1993;262:2005–2009.
59. Branca RT, Capuani S, Maraviglia B. About the crazed sequence. *Concepts Magn Reson A* 2004;21A:22–36.
60. Richter W, Warren WS. Intermolecular multiple quantum coherences in liquids. *Concepts Magn Reson* 2000;12:396–409.
61. Zhong JH, Chen Z, Kwok E. In vivo intermolecular double-quantum imaging on a clinical 1.5 T MR scanner. *Magn Reson Med* 2000;43:335–341.
62. Rance M. Improved techniques for homonuclear rotating-frame and isotropic mixing experiments. *J Magn Reson* 1987;74:557–564.